

LA-UR -81-1220

CONF - 810424 - 1-1

MASTER

TITLE: RADIAL-PULSE PROPAGATION AND IMPEDANCE CHARACTERISTICS OF OPTICALLY SHUTTERED CHANNEL INTENSIFIER TUBES

AUTHOR(S):

J. L. Detch, Jr.*

B. W. Noel

SUBMITTED TO:

Los Alamos Conference on Optics '81

DISCLAIMER

This document is the property of the United States Government and is loaned to your organization; it and its contents are not to be distributed outside your organization.

*EG&G, Inc., Santa Barbara Operations, 130 Robin Hill Road, Goleta, CA 93017

By acceptance of this article, the publisher recognizes that the U.S. Government retains a nonexclusive, royalty free license to publish or reproduce the published form of this contribution, or to allow others to do so, for U.S. Government purposes.

The Los Alamos Scientific Laboratory requests that the publisher identify this article as work performed under the auspices of the U.S. Department of Energy.

University of California



LOS ALAMOS SCIENTIFIC LABORATORY

Post Office Box 1663 Los Alamos, New Mexico 87545

An Affirmative Action/Equal Opportunity Employer

B405

Radial-pulse propagation and impedance characteristics of optically shuttered
channel intensifier tubes

J. L. Detch, Jr.
EG&G, Inc., Santa Barbara Operations
130 Robin Hill Road, Goleta, California 93017
and
B. W. Noel
Los Alamos National Laboratory
MS 678, P. O. Box 1663, Los Alamos, New Mexico 87545

Abstract

Electrically gated proximity-focused channel intensifier tubes are often used as optical shutters. Optimum nanosecond shuttering requires both understanding the electrical pulse propagation across the device structure and proper impedance matching. A distributed-transmission-line model is developed that describes analytically the voltage- and current-wave propagation characteristics as functions of time for any point on the surface. The optical gain's spatial uniformity and shutter-open times are shown to depend on the electrical pulse width and amplitude, and on the applied bias. The driving-point impedance is derived from the model and is expressed as a function of an infinite sum of terms in the complex frequency. The synthesis in terms of lumped-constant network elements is realized in first- and second-Foster equivalent circuits. Experimental impedance data are compared with the model's predictions and deviations from the ideal model are discussed.

Introduction

The basic active components of proximity-focused channel intensifier tubes** include a glass faceplate on which a photocathode is formed, followed by a microchannel plate (a fused bundle of 12.5- μ m-diam hollow glass tubes, or microcapillaries) and an output fiber-optic window on which a phosphor is formed. Biasing electrical connections are made to the photocathode, the input and output ends of the microchannel plate (MCP), and the phosphor anode. Photoelectrons emitted from the photocathode that enter the microcapillaries are accelerated by the applied potential, strike the walls, and are multiplied by secondary emission, producing an electron cascade. Electronic gains from a few hundred to a few thousand may be obtained in this manner. The electron gain of the MCP varies as a function of the voltage applied across it. Upon exiting the MCP capillaries, the electrons are further accelerated into the phosphor, thereby producing the intensified image. The intensifier may be shuttered off by operating the MCP input at reverse bias relative to the photocathode so that photoelectrons cannot reach the MCP input. The intensifier can then be gated on by applying a forward-biasing pulse. We refer to the set consisting of the photocathode, the MCP input, and the gap between them as the MCP gate.

Experimental evaluation of gated intensifier tubes has revealed several interesting phenomena. First, when a fast turn-on pulse is applied to the MCP gate, the gain of the intensifier progresses radially inward at a nonlinear rate. Second, applied potential differences that are sufficient to completely turn on the intensifier in the steady state may only partially turn it on in the pulsed mode. Under this condition, the region having optical gain progresses radially inward, but may not reach the center of the intensifier before pulse extinction occurs. Third, the turn-on characteristic generally progresses radially inward, followed some time later by a turn-off characteristic that progresses radially inward in a time that may significantly exceed the FWHM of the driving pulse. Fourth, the rate of turn-off (radius versus time) may not exhibit the same behavior as the rate of turn-on.

A mathematical model is developed that describes all of these turn-on phenomena. The describing equations are put into a form that uses dimensionless parameters. This form enables one to characterize and compare various intensifier configurations. We start with a distributed resistive-capacitive model of the MCP gate and derive from it the describing

*This work was performed under the auspices of the U.S. Department of Energy. The EG&G portion was supported by Department of Energy contract no. DE-AC08-76NV01183 for the Los Alamos National Laboratory.

**Often called proximity-focused microchannel-plate image intensifiers.

B405

differential equation. The differential equation is solved and matched to the boundary conditions for a step-function input. A set of universal turn-on curves is generated for a step-function input. The curves allow one to characterize any intensifier in terms of its radius and a propagation constant that is determined by either the network's sheet resistance and capacitance or the turn-on time.

The knowledge of the potential everywhere across the MCP gate as a function of radius and time after initiation of the step-function input is used to develop the equivalent response to an impulse (delta-function) input. The MCP-gate response to an arbitrary driving function is obtained from the impulse response by convolution.

Proper electrical impedance matching is required at the MCP gate in order to minimize reflected gating-pulse energy, to get the fastest risetime, and to have the best waveform in fast-pulse applications. To accomplish impedance matching will require a suitable equalizing circuit between the pulse source and the MCP gate, because the intensifier alone is not a good impedance match. To design equalizing networks requires detailed knowledge of the driving-point-impedance characteristics of the MCP gate. The model permits calculating the driving-point impedance. The current across and through the MCP gate as a function of radius and time is calculated from the potential. The Laplace transforms of the potential and current functions are calculated. The ratio of these two s-plane functions yields an analytical expression for the complex impedance of the MCP gate as a function of radius and frequency. When the expression is evaluated at the perimeter radius, one obtains the driving-point impedance.

The model shows excellent general agreement with the observed phenomena and is consistent with the basic electrical behavior. At least one unexplained optical characteristic has been observed. Under certain operating conditions, the turn-on radius has been seen to propagate radially inward, reverse itself before reaching the center, or complete turn-on, and then return radially outward. The R-C model chosen for this study produces only radially inward-propagating solutions in terms of integer-order Bessel functions. The L-C model of a radial transmission line¹ gives both radially inward- and outward-propagating solutions in terms of Hankel functions. We believe that a combined R-C-L MCP-gate model would yield a description of the observed outward-propagating phenomenon. Unfortunately, the boundary conditions for such a model are difficult to apply. Several electrical phenomena are not now included in the R-C model. For some intensifiers, there is an unexplained decreasing equivalent series resistance (esr) at low frequency. There is also a series resonance partly caused by lead inductance and a parallel resonance from parasitic capacitance. The rest of the series resonance and the esr may perhaps be partly explained with the proposed R-C-L model.

Distributed network model of the MCP gate

We assume that the MCP input and the photocathode are planar with circular symmetry and that the perimeters of these elements are driven simultaneously and symmetrically. As a pulse propagates radially inward, we examine a symmetric ring, of radial thickness dr , located at the radius r . The resistance between the inner and outer edges of the ring is

$$\rho(r)dr = \frac{\rho_0}{2\pi r} dr, \quad (1)$$

where ρ_0 is the combined sheet resistance of the photocathode and MCP input, and $\rho(r)$ is the resistance per unit width.

We then consider the elemental parallel-plate capacitor formed by the photocathode ring, the adjacent ring on the MCP input surface, and the gap. We obtain a capacitance that is proportional to the radius:

$$C(r)dr = 2\pi C_A dr, \quad (2)$$

*There appear to be some conditions where the latter assumption does not hold, but we do not consider them here.

B405

where C_a is the capacitance per unit area associated with the photocathode gap. Note that this quantity may be experimentally estimated by measuring the gap capacitance and dividing by the photocathode surface area. Thus, $C_a = C_0/a^2$, where C_0 is the (measurable) total capacitance between the photocathode and the MCP input leads.

With this model for the distributed resistance and distributed shunt capacitance of the MCP-gate structure, we then examine a differential section of radial transmission line located between r and $r + dr$, as shown in Fig. 1. The change in voltage across the element is given by Ohm's law,

$$\frac{\partial v}{\partial r} dr = \rho(r) i dr. \quad (3)$$

Similarly, the change in the current is given by

$$\frac{\partial i}{\partial r} dr = -C(r) dr \frac{\partial v}{\partial t}. \quad (4)$$

The differential radii may be removed from Eqs. (3) and (4) to provide

$$\frac{\partial v}{\partial r} = -\rho(r) i \quad (5)$$

and

$$\frac{\partial i}{\partial r} = -C(r) \frac{\partial v}{\partial t}. \quad (6)$$

We then take the radial partial derivative of Eq. (5) and combine the result with Eqs. (5) and (6). Substituting the explicit forms of the distributed resistance and capacitance from Eqs. (1) and (2), and their derivatives, gives

$$\frac{\partial^2 v}{\partial r^2} = \frac{\rho_0}{r} C_a r \frac{\partial v}{\partial t} - \frac{r}{\rho_0} \frac{\rho_0}{r^2} \frac{\partial v}{\partial r}, \quad (7)$$

which reduces to

$$\frac{\partial^2 v}{\partial r^2} + \frac{1}{r} \frac{\partial v}{\partial r} - \frac{1}{K} \frac{\partial v}{\partial t} = 0 \quad (\text{for } 0 < r < a), \quad (8)$$

where $K = 1/\rho_0 C_a$ is a propagation constant and a is the perimeter radius of the MCP gate. The particular solution of Eq. (8) may be shown to be of the form

$$v(r, t) = A J_0(\alpha r) e^{-K\alpha^2 t}, \quad (9)$$

where J_0 is the Bessel function of the first kind of order zero.

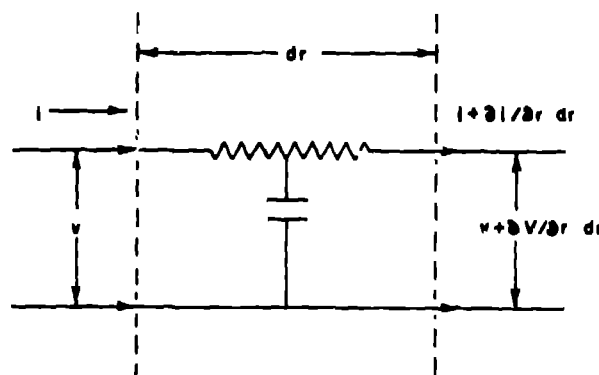


Fig. 1. Differential distributed transmission line representing two adjacent elemental rings on the MCP gate structure.

B405

Solution for a step-function input

Assume that we apply a step-function voltage of amplitude V_0 to the perimeter of the MCP gate at a time $t = 0$ and maintain the perimeter voltage $v(a, t) = V_0$ for all subsequent time. Then Eq. 9 must be modified by an additive constant (or constants) determined from the roots of

$$J_0(\alpha_n a) = 0. \quad (10)$$

The general solution becomes

$$v(r, t) = V_0 + \sum_{n=1}^{\infty} A_n J_0(\alpha_n r) e^{-K\alpha_n^2 t}. \quad (11)$$

Examining the boundary condition at $t = 0$, when the potential elsewhere across the MCP gate is assumed to be zero, we obtain the relationship

$$\sum_{n=1}^{\infty} A_n J_0(\alpha_n r) = -V_0 \quad (\text{for } 0 < r < a). \quad (12)$$

The orthogonality relations for the J_0 Bessel functions are given by

$$\int_0^a r J_0(\alpha_m r) J_0(\alpha_n r) dr = \begin{cases} 0 & \text{for } m \neq n \\ \frac{1}{2} a^2 J_1^2(\alpha_n a) & \text{for } m = n \end{cases}. \quad (13)$$

This relationship may be exploited to solve for the factors A_n to yield the potential across the MCP gate as a function of the radius and time,

$$\frac{v(r, t)}{V_0} = 1 - \frac{2}{a} \sum_{n=1}^{\infty} e^{-K\alpha_n^2 t} \cdot \frac{J_0(r\alpha_n)}{\alpha_n J_1(\alpha_n a)}. \quad (14)$$

For comparing gated MCP image intensifiers having different physical parameters, it has been found convenient to express Eq. (14) in a dimensionless (universal) form in terms of the fractional radius, r/a , and a universal time parameter, $T = Kt/a^2$, where t is the laboratory time. Using these dimensionless parameters, Eq. (14) may be written as

$$\frac{v(r/a, T)}{V_0} = 1 - 2 \sum_{n=1}^{\infty} e^{-\beta_n^2 T} \frac{J_0((r/a)\beta_n)}{\beta_n J_1(\beta_n)}, \quad (15)$$

where $\beta_n = a\alpha_n$. The reader should note the similarity between this solution and that for radial heat flow in an infinite cylinder, as solved by Carslaw and Jaeger.⁴ The internal rise of potential of the MCP gate following application of a step function is shown in Fig. 2 in terms of fractional potential vs fractional radius for various values of the universal time parameter. Note that an arbitrary bias may be added and the time required for a given radius to reach a specified potential may be readily determined.

B406

Solution for a delta-function input

Applying Duhamel's theorem allows one to differentiate Eqs. (14) or (15) with respect to time to produce the corresponding impulse response for a delta function of potential applied at $t = 0$. The response may be expressed in terms of laboratory or dimensionless time, respectively, by

$$H(r,t) = \frac{2K}{a} \sum_{n=1}^{\infty} a_n e^{-Ka_n^2 t} \frac{J_0(r/a_n)}{J_1(a_n)} \tag{16}$$

or

$$H(r/a,T) = 2 \sum_{n=1}^{\infty} \beta_n e^{-\beta_n^2 T} \frac{J_0((r/a)\beta_n)}{J_1(\beta_n)} \tag{17}$$

The dimensionless form, Eq. (17), of the impulse response is shown in Fig. 3 for the same values of the universal time parameter as shown in Fig. 2 for a step-function input. Note in particular that an impulse does not readily propagate across the MCP gate without serious degradation.

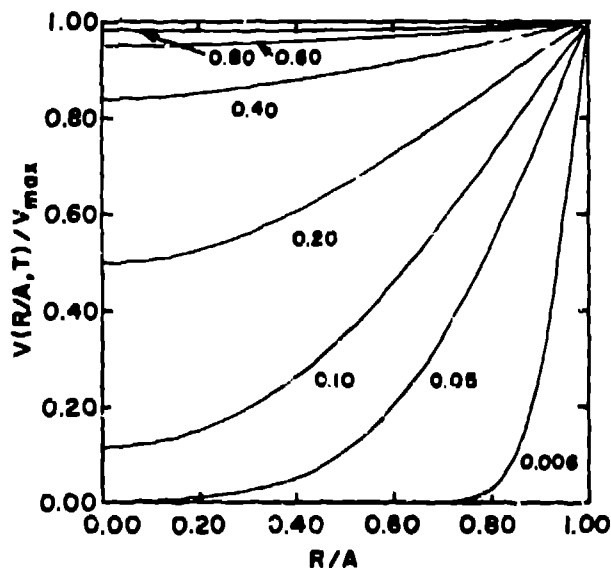


Fig. 2. Universal turn-on curves for step-function input, showing fractional potential excursion vs fractional radius for values of the time parameter, T , between 0.006 and 0.80.

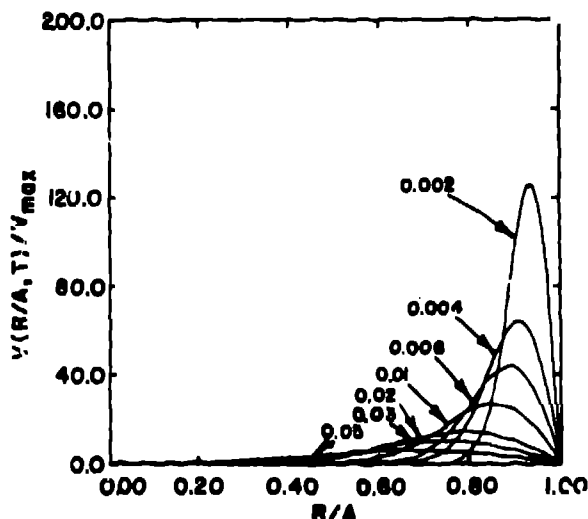


Fig. 3. Universal turn-on and turn-off curves for impulse input for values of T between 0.002 and 0.05. Vertical scale is normalized to unit area under curve at $T=0$.

Solution for an arbitrary input function

The propagating potential across the MCP gate for an arbitrary input function $X(t)$, is given by the causal convolution integral

$$v_X(r,t) = \int_0^t X(\tau) H(r,t-\tau) d\tau \tag{18}$$

As an example of this operation, consider as an input function the causal first-moment exponential pulse given by

$$X(t) = \begin{cases} 0 & t < 0 \\ Ate^{-\gamma t} & 0 < t \end{cases}, \tag{19}$$

where γ is related to $t_{1/2}$, the FWHM of the driving pulse, by $\gamma = 2.44639/t_{1/2}$, and the constant, A , is related to the peak voltage excursion, X_{max} , by the relationship $A = X_{max}\gamma e^{\gamma t_{1/2}}$. Integration of Eq. (18) with Eq. (19) as the input function yields the result

$$v_1(r,t) = \frac{2KA}{a} \sum_{n=1}^{\infty} \frac{J_0(r\alpha_n)}{J_1(a\alpha_n)} \frac{e^{-K\alpha_n^2 t}}{(K\alpha_n^2 - \gamma)^2} \left\{ e^{(K\alpha_n^2 - \gamma)t} \left[(K\alpha_n^2 - \gamma)t - 1 \right] + 1 \right\}. \tag{20}$$

As an example of the behavior of Eq. (20), assume that a MCP gate has a radius of $a = 0.5$ cm, is biased off at -40 V, turns on when the potential across the gap exceeds zero, and is completely turned on in 1 ns after a step-function excursion to $+160$ V is applied. This corresponds to a value of the propagation constant, $K = 2.02 \times 10^{-2}$ cm²/ns. Assume the driving pulse is of the form of Eq. (19), has a FWHM of $t_{1/2} = 1$ ns, and reaches a peak potential of $+160$ V (200 V above the assumed -40 -V bias). Then Eq. (20) gives the results shown in Fig. 4. Note the initial inward-propagating rise in potential until the entire intensifier is turned on, followed by an inward-propagating decrease in potential that subsequently turns off the tube. The time between adjacent curves is 0.2 ns. The times of crossing-zero potential and the corresponding radii for turn-on and turn-off are shown in Fig. 5. Note in particular that the central portion of the intensifier is turned on for significantly greater time than is the perimeter, and that both of these times exceed the FWHM of the driving pulse.

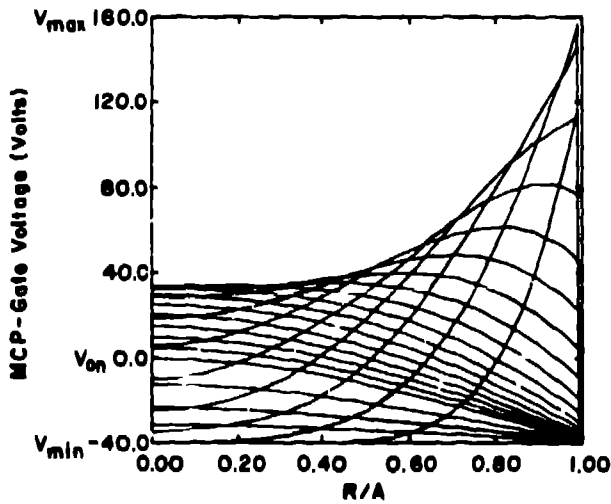


Fig. 4. MCP gate voltage as function of time and position as calculated from Eq. (20) with parameters described in text.

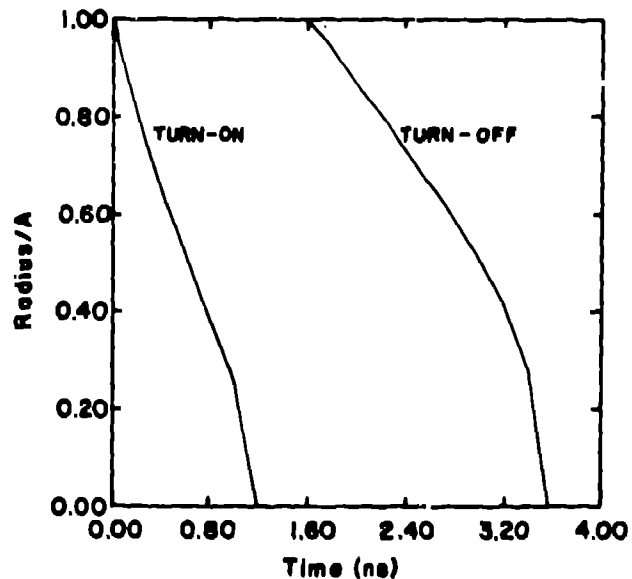


Fig. 5. Turned-on and turned-off radii vs time for the same parameters used in Fig. 4 and described in text.

Calculation of the impedance

The voltage across the MCP gate as a function of radius and time is given by Eq. (14). By combining Eqs. (1) and (3) and taking the radial partial derivative of Eq. (14), we obtain the current as a function of radius and time:

$$i(r, t) = \frac{2\pi r}{\rho_0} \frac{\partial v(r, t)}{\partial r} = \frac{4\pi r V_0}{\rho_0 a} \sum_{n=1}^{\infty} e^{-k_n^2 t} \frac{J_1(r a_n)}{J_1(a a_n)}. \quad (21)$$

The impedance of the radial transmission line as a function of radius is found by taking the ratio of the Laplace-transformed voltage and current,

$$Z(r, s) = \frac{V(r, s)}{I(r, s)} = \frac{\rho_0 a}{4\pi r} \frac{\left[\frac{1}{s} + \frac{2}{a} \sum_{n=1}^{\infty} \frac{J_0(r a_n)}{J_1(a a_n)} \frac{1}{k_n^2 + s} \right]}{\left[\sum_{n=1}^{\infty} \frac{J_1(r a_n)}{J_1(a a_n)} \frac{1}{k_n^2 + s} \right]}. \quad (22)$$

The driving-point impedance is obtained by evaluating Eq. (22) at the edge of the MCP gate, where $r = a$. Thus,

$$Z(a, s) = \frac{\rho_0}{4\pi s} \frac{1}{\sum_{n=1}^{\infty} \frac{1}{s + k_n^2}}, \quad (23)$$

where $k_n = k_n^2 = \frac{1}{a^2} \frac{4\pi \rho_0 C_0}{s}$. The functional dependence on the radius will henceforth be understood, and we will write $Z(s)$ only.

In this form, $Z(s)$ appears to be difficult to interpret in terms of familiar driving-point-impedance concepts that involve lumped circuit elements. Consequently, we search for ways to synthesize it in terms of such elements.

As a first step in the synthesis, it is straightforward to show that $Z(s)$ is positive real by, for example, Talbot's test.⁴ It is thus synthesizable in a number of ways. We have chosen to develop first- and second-Foster R-C syntheses.

Second-Foster synthesis

Equation (23) may be rearranged easily into the form

$$Z(s) = \frac{1}{\sum_{n=1}^{\infty} \frac{1}{\frac{\rho_0 k_n}{4\pi} \frac{1}{s} + \frac{\rho_0}{4\pi}}}. \quad (24)$$

and then the second-Foster R-C synthesis follows by inspection (Fig. 6). In the figure,

$$C_n = \frac{4\pi}{\rho_0 k_n} = \frac{4C_0}{s_n^2} \quad (25)$$

and

$$R = \frac{\rho_0}{4\pi} \tag{26}$$

Note that $C_{n+1} < C_n$, for all n , because $\beta_{n+1} > \beta_n$ for all n and $\beta_1 > 1$. This means that the first s -plane zero of the circuit in Fig. 6 is located at $s = -1/RC_1 = -1/k_n$. For frequencies from zero to the vicinity of $1/2\pi RC_1$, Eq. (23) becomes

$$Z(s) = \frac{\rho_0}{4\pi s} = \frac{1}{C_0 s} = \sum_{n=1}^{\infty} \frac{1}{k_n} \tag{27}$$

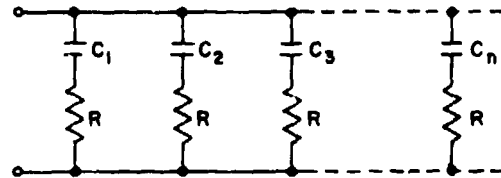


Fig. 6. Second-Foster synthesis of the driving-point impedance.

because

$$\sum_{n=1}^{\infty} \frac{1}{\beta_n^2} = \frac{1}{4} \tag{28}$$

The low-frequency (or first-order) impedance is simply that of the low-frequency capacitance, C_0 , as expected for a correct model. By examining the second-Foster equivalent circuit, we see that the low-frequency capacitance is that due to the infinite number of lumped capacitors taken in parallel; i.e.,

$$\sum_{n=1}^{\infty} C_n = 4C_0 = \sum_{n=1}^{\infty} \frac{1}{\beta_n^2} = C_0 \tag{29}$$

For an 18-mm-diam ITT intensifier, the manufacturer specifies a nominal $\rho_0 = 2000 \Omega$ per square. We measure the low-frequency capacitance to be typically $C_0 = 30.5$ pF. Using these values, the first zero is located at the break frequency $f_1 = 1/2 RC_1 = 47$ MHz. In the region near this frequency, but well below the second break frequency, the circuit is as shown in Fig. 7. For this second-order case, the impedance is then simply $1/sC_{r1} + R$ in parallel with $1/sC_{r1}$, where

$$C_{r1} = \sum_{n=1}^{\infty} C_n - C_1 = C_0 \left(1 - \frac{4}{\beta_1^2}\right) = 0.308 C_0 \tag{30}$$

and $C_{r1} = 6.5$ pF for our 18-mm-diam intensifiers. The foregoing procedure can be repeated to as many elements as are required to cover the bandwidth of the driving circuit. At that point, the lumped-constant circuit should be an excellent approximation to the ideal intensifier with respect to any important properties of the driving source or matching circuits.

The driving-point impedance of any circuit containing only linear lumped elements can be written as the complex sum of an esr and a series reactance. The resistance and reactance are, in general, frequency-dependent, but obviously reduce to constant values at a fixed frequency. For sufficiently low frequencies, the second Foster equivalent circuit reduces to a single capacitor of value C_0 . The series-equivalent components for intermediate frequencies can be found by combining the circuit elements in the usual way. For sufficiently high frequency, $s \rightarrow \infty$, all the capacitors become short circuits and the equivalent network contains only all the equal-valued resistors in parallel. The infinite parallel combination thus reduces to zero resistance and the equivalent series resistance approaches zero as $s \rightarrow \infty$.

B405

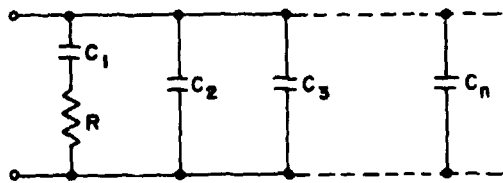


Fig. 7. Second-order version of the second-Foster synthesis.

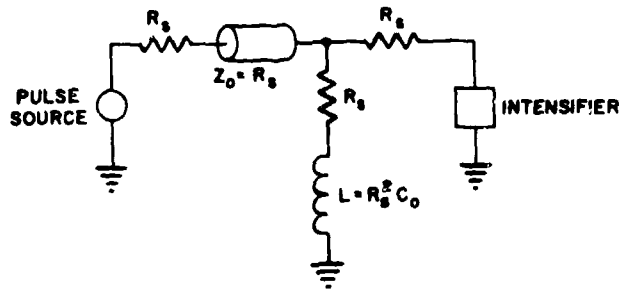


Fig. 8. Properly terminated circuit in frequency region where first-order synthesis is valid.

Consider driving the circuit with a pulse whose risetime corresponds to a frequency below the first breakpoint. In this case, the first-order circuit is an appropriate representation of the intensifier. It is possible to optimize the risetime and waveshape very simply by using a stripline, between the driver and intensifier, whose characteristic impedance equals the output resistance of the driving source. The appropriate stripline termination is shown in Fig 8.⁵ It is also possible to impedance-match by, for example, bridged-tee networks. For operation above the first breakpoint, more-complex matching networks that include equalizers are needed. We note that gating pulses of the order of 1-ns FWHM require operation above the fourth breakpoint. We shall not discuss appropriate matching circuits for such cases here because, as it turns out, parasitics and leakage that are not accounted for in the present model preclude applying them directly.

First-Foster synthesis

The exact form of the first-Foster synthesis cannot be carried out easily. The basic equation for performing it is obtained by observing that, upon collecting terms over a common denominator,

$$\sum_{n=1}^{\infty} \frac{1}{s + k_n} = \frac{\sum_{i=1}^{\infty} \prod_{\substack{n=1 \\ n \neq i}}^{\infty} (s + k_n)}{\prod_{n=1}^{\infty} (s + k_n)}, \quad (31)$$

so that

$$Z(s) = \frac{p_0}{4\pi} \frac{1}{s} \frac{\prod_{n=1}^{\infty} (s + k_n)}{\sum_{i=1}^{\infty} \prod_{\substack{n=1 \\ n \neq i}}^{\infty} (s + k_n)}. \quad (32)$$

The impedance has a pole at $s = 0$ and zeros at each $s = -k_n$. The first zero is at ≈ 47 MHz, as is expected, because this form of the impedance must have the same frequency dependence as that which led to the second-Foster synthesis. The pole at zero can be removed by writing Eq. (32) as

$$Z(s) = \frac{p_0}{4\pi} \left[\frac{A}{s} + F(s) \right], \quad (33)$$

so that, by the theory of residues,

$$A = \frac{\prod_{n=1}^{\infty} (s + k_n)}{\sum_{i=1}^{\infty} \prod_{\substack{n=1 \\ n \neq i}}^{\infty} (s+k_n)} \Bigg|_{s=0} \tag{34}$$

$$= \frac{\prod_{n=1}^{\infty} k_n}{\sum_{i=1}^{\infty} \prod_{\substack{n=1 \\ n \neq i}}^{\infty} k_n} = \frac{1}{\sum_{n=1}^{\infty} \frac{1}{k_n}} = \frac{4\pi}{\rho_0 C_0} \tag{35}$$

Thus

$$Z(s) = \frac{1}{C_0 s} + \frac{\rho_0}{4\pi} F(s) \tag{36}$$

The pole at $s = 0$ comes from a capacitor of value C_0 . The numerator of $F(s)$ is one order lower than that of the denominator, so there is no removable series resistor. This is expected since, as we showed earlier, the value of the esr approaches zero as $s \rightarrow \infty$.

It does not appear to be possible to evaluate $F(s)$ exactly in the form of the partial-fraction expansion needed to complete the synthesis. To do so requires factoring a denominator containing an infinite number of terms in order to find the poles. Each of these gives rise to a parallel R-C element pair. However, we do know the location of all the zeros of $Z(s)$ from Eq. (32). It can be shown that the poles and zeros of this function alternate, so we may be able to make a useful approximation to the location of any pole by say, taking the logarithmic average of the two adjacent zeros. The final network will be of the form shown in Fig. 9.

Approximate first-Foster synthesis

An approximate first-Foster R-C synthesis can be realized. The main advantage of it is that one can calculate the exact values of the components. The disadvantage is that the approximation improves only as the number of components increases, and the latter increase causes a manifold increase in the algebraic complexity of the calculations.

The procedure used is to truncate the series in Eq. (32) after n terms and perform the algebra required to put the truncated $Z(s)$ into the proper form for first-Foster synthesis. The results are illustrated in Fig. 10. In this figure,

$$R_n = \frac{\rho_0}{4\pi} \frac{1}{n} \tag{37}$$

and

$$C_n = \frac{4\pi}{\rho_0} \prod_{j=1}^n \frac{1}{k_j} \tag{38}$$

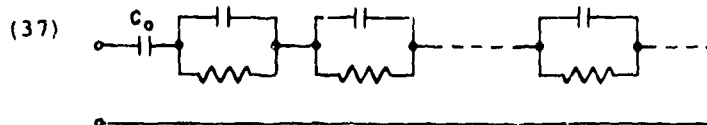


Fig. 9. First-Foster synthesis of the driving-point impedance.

Note that $R_n \rightarrow 0$ as $n \rightarrow \infty$, as it should, based on our earlier discussion. Similarly, C_n increases toward a constant value, namely C_0 , for $n \rightarrow \infty$.

The parallel components for $n = 2$ are

$$R_p = \frac{\rho_0}{8\pi} \frac{k_1^2 + k_2^2}{(k_1 + k_2)^2} \quad (39)$$

and

$$C_p = \frac{16\pi}{\rho_0} \frac{k_1 + k_2}{k_1^2 + k_2^2} \quad (40)$$

The expression for the values of the parallel elements is extremely complicated for $n > 3$. For $n = 3$, the element values are

$$R_3 = \frac{\rho_0}{12\pi} \quad (41)$$

$$C_3 = \frac{4\pi B}{\rho_0 C} \quad (42)$$

$$R_{p1} = \frac{\rho_0}{4\pi} \frac{(AB-9C)(\sqrt{A^2-3B-A}) + 6(B^2-3AC)}{6B(A\sqrt{A^2-3B} - (A^2-3B))} \quad (43)$$

$$C_{p1} = \frac{4\pi}{\rho_0} \frac{18B\sqrt{A^2-3B}}{(AB-9C)(\sqrt{A^2-3B-A}) + 6(B^2-3AC)} \quad (44)$$

$$R_{p2} = \frac{\rho_0}{4\pi} \frac{(AB-9C)(\sqrt{A^2-3B+A}) - 6(B^2-3AC)}{6B(A\sqrt{A-3B} + (A-3B))} \quad (45)$$

and

$$C_{p2} = \frac{4\pi}{\rho_0} \frac{18B\sqrt{A^2-3B}}{(AB-9C)(\sqrt{A^2-3B+A}) - 6(B^2-3AC)} \quad (46)$$

where $A = k_1 + k_2 + k_3$, $B = k_1k_2 + k_1k_3 + k_2k_3$, and $C = k_1k_2k_3$. For our intensifiers, we calculate that $R_3 = 53 \Omega$, $C_3 = 26.8 \text{ pF}$, $R_{p1} = 41 \Omega$, $C_{p1} = 28.5 \text{ pF}$, $R_{p2} = 10 \Omega$, and $C_{p2} = 34.6 \text{ pF}$. For this case, each additional capacitor is increased in value, as expected, because the capacitors are in series. The three time constants are $R_3C_3 = 1.4 \text{ ns}$, $R_{p1}C_{p1} = 1.2 \text{ ns}$, and $R_{p2}C_{p2} = 0.35 \text{ ns}$. Since any additional component pairs have time constants shorter than R_3C_3 , and since we are interested in gating on the tubes for times $\sim 1 \text{ ns}$, it appears that the given three-time-constant circuit may be adequate as an approximation to the ideal MCP-gate equivalent circuit.

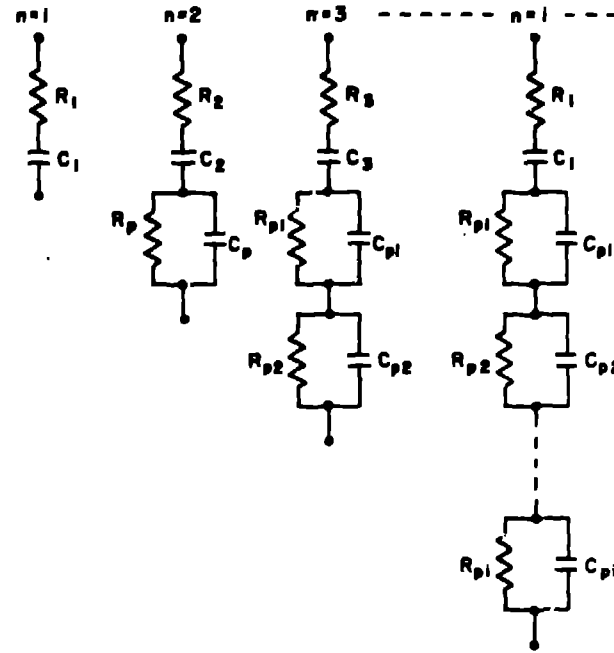


Fig. 10. Approximate first-Foster networks for the truncated driving-point impedance.

Electrical measurements

The driving-point impedance was measured by one or more of several methods for each of six ITT tubes. Impedance data were obtained at various frequencies. Our intent was to compare the measured impedance with that predicted by the model as a function of frequency.

Measurements were made at 1, 4, and 10 MHz with a Hewlett-Packard model 4275A LCR meter. A Hewlett-Packard model 3042A Automatic Network Analyzer was configured to measure reflectance. The data were taken quasi-continuously over the range from 1 to 13 MHz. The devices were measured extensively at selected spot frequencies from 1 to 500 MHz with a Hewlett-Packard model 4191A rf Impedance Analyzer. It was found generally that the measurements made below 10 MHz by the first two methods, and below 3 MHz by the third, were too noisy to permit accurately evaluating the esr. The data obtained by the three methods generally agreed well. A summary of the data at 10 MHz is given in Table I.

TABLE I

Summary of Equivalent Series Resistance
and Capacitance Data on ITT Intensifier Tubes at 10 MHz

| Intensifier Serial Number | C_m | C_A | C_z | R_m | R_A | R_z |
|---------------------------------|-------|-------|-------|-------|-------|-------|
| 788/1 | 29.7 | 31.7 | 31.3 | 64 | 54 | 64.3 |
| 787/1 | -- | 31.1 | 30.7 | -- | 43 | 59.7 |
| 787/3 | -- | 26.7 | 30.2 | -- | 48.5 | 50.9 |
| 787/10 | 29.6 | 30.5 | 29.8 | 4.1 | 10.3 | 10.1 |
| 788/7 | -- | 28 | -- | -- | <10 | -- |
| 788/6 | -- | 34.9 | -- | -- | 12.5 | -- |

C_m, R_m = data measured with LCR meter

C_A, R_A = data measured with automatic network analyzer

C_z, R_z = data measured with rf impedance analyzer

The best data are thought to be those from the 4191A. Using this instrument, the measured capacitance for four of the tubes was 30.5 ± 0.8 pF. The small spread verifies that the device dimensions vary little in manufacturing; the tested tubes came from two different batches.

The measured esr varies greatly among tubes. Independent turn-on measurements⁶ show that those with the lowest esr tend to turn on fastest. We have so far been unable to directly relate the measured esr to the calculated value. The ideal model shows a constant esr in the region below the first breakpoint. Experimentally, for some devices, the esr is constant over a wide frequency range below the first calculated breakpoint. For other, it is inversely proportional to frequency. Several factors could contribute to this and other observed anomalies. First, we know that the photocathode resistivity varies among intensifiers for several reasons. Second, the measured esr includes contributions from the parallel ac-leakage resistance and other parasitics not included in the model, such as stray capacitance and lead inductance. Third, it may be necessary to include the effects of distributed inductance to account fully for the observed esr as well as for the turn-on anomalies discussed earlier.

The esr for five intensifiers is plotted in Fig 11. In several cases the esr is proportional to about $f^{-1.2}$. The relationship would be f^{-2} for a purely resistive leakage in parallel with the tube. Such a leakage would have to have a value of 4.6 k Ω to agree with typical measured values of esr, whereas we estimate the low-frequency leakage resistance to be 300 M Ω .

The broadband data obtained with the rf impedance analyzer show additional effects that are not accounted for by the idealized model. Figure 12 is a plot of the magnitude of the impedance as a function of frequency for a tube exhibiting constant esr below the first breakpoint. A series resonance occurs at 175 MHz. Its effect over a broad range of frequencies masks evidence, if there is any, of the breakpoint that should occur at ≈ 47 MHz if the estimated ρ_0 is the correct value. The series resonance is caused partly by the lead inductance resonating with the device capacitance. The required inductance is 27 nH.

The estimated maximum lead inductance, given the physical layout and dimensions, is about 16 nH. The proposed refinements to the model will have to account for this effect.

There is a small parallel resonance at about 350 MHz. It is caused by the aforementioned inductance resonating with the stray capacitance.

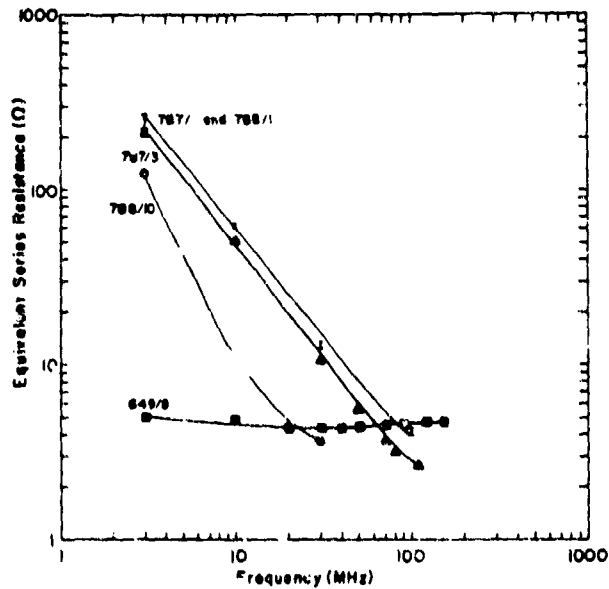


Fig. 11. Measured equivalent series resistance for five intensifier tubes.

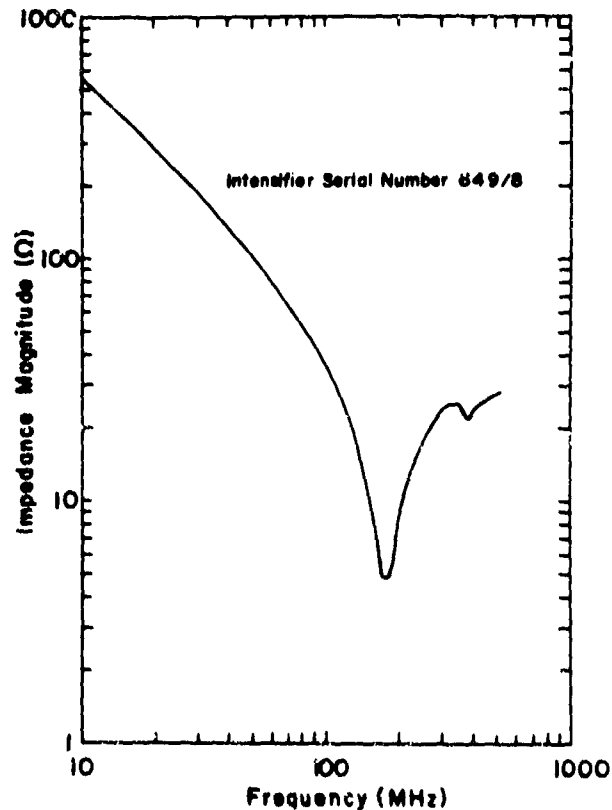


Fig. 12. Amplitude of the impedance vs frequency for one intensifier tube.

References

1. S. Ramo and J. R. Whinnery, Fields and Waves in Modern Radio (John Wiley and Sons, New York, 1947).
2. H. S. Carslaw and J. C. Jaeger, Conduction of Heat in Solids, Second edition (Oxford University Press, Oxford, 1959).
3. J. L. Detch, Jr., and J. W. Ogle, "A Distributed R-C Radial Transmission Line Theory Applied to the Gain Characteristics of Gated Microchannel-Plate Image Intensifiers," EG&G report EGG 1183-2404 (June 1980).
4. A. Talbot, "A New Method of Synthesis of Reactance Networks," Proc. IEE (London) 101, 73-90 (1954).
5. R. E. Partridge, Los Alamos National Laboratory, personal communication.
6. G. J. Yates, Los Alamos National Laboratory, unpublished data.